

Numerical and Experimental Study of Geometrical Dimensions on Laser-TIG Hybrid Welding of Stainless Steel 1.4418

Mahmoud Moradi^{1*}, Majid Ghoreishi², Azam Rahmani²

¹Department of Mechanical Engineering, Faculty of Engineering, Malayer University, Malayer, Iran

²Faculty of Mechanical Engineering, K.N. Toosi University of Technology, Tehran, Iran

*Email of Corresponding Author: moradi.malayeru@gmail.com

Received: May 24, 2016; Accepted: August 5, 2016

Abstract

In this paper, a three-dimensional finite element model has been developed to simulate the laser-TIG hybrid welding (HLAW) of stainless steel 1.4418 with thickness of 4 mm. Transient temperature profile and dimensions of the fusion zone and heat affected zone (HAZ) during welding process are calculated using finite element method (FEM) and were solved in the ABAQUS/Standard software. The heat source model is a combination of Goldak distribution for the arc heat flux, a body Gaussian distribution for laser heat flux and a surface heat flux model. The DFLUX subroutine was used for implementation of the movable welding heat sources of the models. To validate the model, several HLAW experiments were performed with a pulsed Nd:YAG laser and TIG sources. Good agreement between the simulated and the experimental measurements revealed that the model would be appropriate for HLAW numerical simulation. Among the material properties, the material conductivity is the most important term which influences on the weld bed dimensions.

Keywords

Laser-TIG Hybrid Welding, Temperature Field, FEM-Simulation- Nd:YAG Laser, Heat Source Model

1. Introduction

Laser-arc hybrid welding, which combines laser welding and arc welding techniques, was originally invented for combined laser-TIG welding [1]. Both laser welding and arc welding processes create plasma, thus lead to a highly complex physical situation. Combination of a laser beam and an electric arc has several advantages versus pure laser welding or arc welding such as: higher processing speeds, deeper penetration, greater tolerance to fit-up, low distortion, welding process stability and efficiency [2-4].

A general review and complete bibliography of laser hybrid processes are prepared by Bagger and Olsen [2]. Pulsed Nd:YA Glaser welding of AISI 304 stainless steel plate was simulated using commercial finite element software to determine the optimal welding conditions by Kim et al. [5]. Wang et al. [6] investigated the interaction between laser-induced plasma/vapor and arc plasma during fiber laser-MIG hybrid welding. Hee et al. [7] were studied and evaluated the effects of welding process (CO₂ laser-GMA hybrid welding and SAW) on the temperature distribution and welding residual stresses of welded joints. Optimization of bead geometry in CO₂ laser welding of Ti 6Al 4V using response surface method is investigated by khorram et al. [8]. Moradi et al. [9]

analyzed the stability of the resulting weld surface appearance and in turn of the welding process for fiber laser-MAG hybrid welding of stainless steel by the aid of design of experiments and high speed imaging. Javid et al. [10, 11] studied a three-dimensional heat transfer simulation of the laser welding process by thermo-mechanical analysis using finite element method. Thermal elastic-plastic analysis by using finite element method to investigate the thermo mechanical behavior and evaluate the residual stresses and welding distortion on the AZ31B magnesium alloy and 304L steel butt joints in HLAW was described in the Zeng et al. research [12] Cerit et al. [13] surveyed stress concentration effects of undercut defects and reinforcement of metals in butt welded joints using the finite element method. Cho et al. [14] studied the physical assumptions and mathematical models required to predict molten metal flow precisely in CO₂ laser-GMA hybrid welding. In hybrid laser-TIG welding processes modeling, Chen et al. [15] analyzed the heat transfer mechanism, and simulated the heat transfer and energy interaction mechanism. Kong and Kovacevic [16] developed a three dimensional (3D) finite element model to investigate thermally induced stress field during hybrid fiber laser-gas tungsten arc welding (GTAW) process. Deng [17] investigated the effects of solid state phase transformation on welding residual stress and distortion in low carbon and medium carbon steels based on finite element model. The applications of lasers in industries are increasing recently. Using laser energy for welding technology to join steel, Ti6-4 and other applicable materials in aerospace industries are widely used in researches and industry [18, 19]. Hybrid arc-laser welding is another new technology which is used for joining thick materials when the laser cannot penetrate completely [20]. Creating micro holes on the sheet using laser beam is another application of laser which is called laser drilling [21, 22].

In the present study, numerical and experimental study of geometrical dimensions on low power Nd:YAGHLAW of martensitic stainless steel 1.4418 with the thickness of 4mm was investigated. Cross section of a typical experimental welding sample was measured to investigate the geometrical dimensions of weld-bead profile and to compare with the simulated results. Thermal elasto- plastic analysis was performed using finite element techniques to analyze the thermo mechanical behavior of butt joint weld by commercial software named ABAQUS. Good agreement between the simulated and the experimental measurements revealed that the model would be appropriate for LHAW numerical simulation.

2. Experimental Procedure

In this study, stainless steel 1.4418 sheets (254mm × 38mm) with thickness of 4 mm were used as the material work piece which is used in the compressor shaft of the gas turbines. The chemical composition of the material, which is the average of three X-ray fluorescence (XRF) measurements, is presented in Table 1.

Table 1. Chemical composition of Stainless steel 1.4418 (wt %)

Fe	Cr	Ni	Mo	Mn	Cu	Si	W	Al	V	C	Co	P	S
Bal	15.91	4.89	0.86	0.72	0.22	0.21	0.15	0.10	0.11	0.037	0.035	0.023	0.005

In the experiments, a pulsed Nd:YAG laser model IQL-10 with a maximum mean laser power of 400 W was used as a laser source combined with a direct current electrode negative TIG (DCEN-

TIG) which are with a maximum current of 250 amperes. Square shape pulses are the standard output of this laser machine. The available range for the laser parameters was 1–1000 Hz for pulse frequency, 0.2–20 ms for pulse duration, and 0–40 J for pulse energy. Since the average laser power could not be more than 400W, it is evident that no arbitrary combination of pulse energy and pulse frequency could be used. The focusing length of laser beam was 75 mm with 250 μm minimum spot size. A 5000W-Lp Ophir power meter and LA300W-LP joule meter were used to measure average power and pulse energy. Details of the experimental setup can be found in [18, 19]. Figure 1 shows the principle of the HLAW process. As shown in this Figure, the arc is leading, no filler metal is used and the laser is vertical to the base metal and the TIG torch is placed with a 35 degree angle to the horizontal surface. The diameter of a tungsten electrode was 1.2 mm. Fixed process parameters, which are the results of author's previous study [23, 24], are presented in Table 2. Before welding, the grease and residue on the surface of the base metal were removed with acetone; beside of it, the oxidation film was removed with stainless steel brush. In the previous author's research [23], HLAW was conducted using RSM as a statistical design of experiments. Welding speed (S), TIG Current (I) and distance of heat sources (D_{LA}) [25] were considered as input process parameters while welding surface width (W), pool area (A), and penetration (P) were the three process responses. Optimization of the HLAW parameters was carried out in order to access minimum geometrical dimensions of weld-bead profile and full penetrated weld according to achieved mathematical models. In the present work, the optimum parameters of the experiment, which obtained from the previous study [23] are mentioned in Table 2.

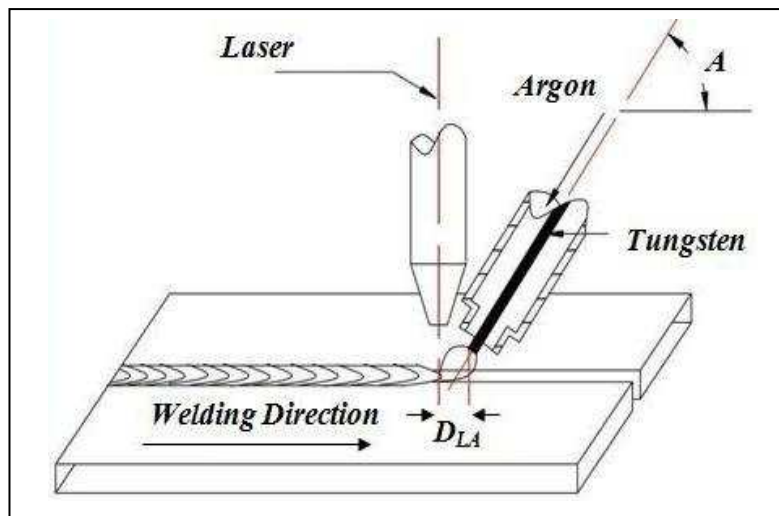


Figure1. Schematic drawing of laser-TIG hybrid welding (arc leading)

Table2. Optimum parameters of study

Parameter	Value
Focal plane position	+2 mm
Shielding gas pressure of laser	25 l/min
Shielding gas (Argon) pressure of TIG	15 l/min
Pulse duration	6 ms
Laser beam frequency	12 Hz
Pulse energy	16.6 J
Torch angle (from the surface)	35°
tungsten electrode stick out length	15 mm
Welding speed	2.5mm/s
Distance of heat sources	2mm
Voltage of ARC	20 V
Current of TIG source	130 A

3. Finite Element Modeling

3.1 Governing Equations and Boundary Conditions

The welding process has high nonlinear transient state. In the heat transfer analysis, the transient temperature field T of the laser welded sheet is a function of time t and the spatial coordinates (x, y, z) and is determined by the non-linear heat transfer equation. The governing partial differential equation for the transient heat conduction is given by [26]

$$\frac{\partial}{\partial x} \left(k_x(T) \frac{\partial T}{\partial x} \right) + \frac{\partial}{\partial y} \left(k_y(T) \frac{\partial T}{\partial y} \right) + \frac{\partial}{\partial z} \left(k_z(T) \frac{\partial T}{\partial z} \right) + Q(x, y, z, t) = \rho(T)c(T) \frac{\partial T}{\partial t} \quad (1)$$

where x, y and z refer to the Cartesian coordinates and Q, the internal heat generation, ρ(T), the temperature dependent density, c(T), the temperature dependent specific heat, and K_x(T), K_y(T) and K_z(T), the temperature dependent thermal conductivity in x, y and z direction respectively. For an isothermal material the equation will be

$$\frac{\partial}{\partial x} \left(k \frac{\partial T}{\partial x} \right) + \frac{\partial}{\partial y} \left(k \frac{\partial T}{\partial y} \right) + \frac{\partial}{\partial z} \left(k \frac{\partial T}{\partial z} \right) + Q = \rho c \frac{\partial T}{\partial t} \quad (2)$$

Matrix form of equation (2) can be written as equation (3)

$$(L)^T (D\{L\}T) + Q = \rho c \frac{\partial T}{\partial t} \quad (3)$$

Where,

$$L = \begin{bmatrix} \frac{\partial}{\partial x} \\ \frac{\partial}{\partial y} \\ \frac{\partial}{\partial z} \end{bmatrix} \quad (4)$$

And

$$D = \begin{bmatrix} k & 0 & 0 \\ 0 & k & 0 \\ 0 & 0 & k \end{bmatrix} \quad (5)$$

Let for any element E, the temperature is represented by equation 6

$$T = [N]T_E \quad (6)$$

T_E is nodal temperature and $[N]$ is the matrix of element shape function.

The temperature fields in thermal analysis fields can be obtained from equation 6. Those results further can be used for structural response (stress / strain fields) in mechanical (structural) analysis. A system of equations is obtained by assembling the individual elemental equation, and is solved for the unknown nodal temperatures T_E .

From the theory of basic solid mechanic $\sigma=D\varepsilon^{el}$ and $\varepsilon=\varepsilon^{el} + \varepsilon^{th}$ where, ε is total Strain, ε^{el} is Elastic Strain, ε^{th} is thermal strain and D is the material stiffness.

The thermal strain vector for an isotropic medium with temperature dependent coefficient of thermal expansion is given as

$$\varepsilon^{th} = \Delta T\alpha(T) \quad (7)$$

Where, ΔT is the difference between the reference temperature and actual temperature.

A part of absorbed energy is transferred from the metal to the environment by convection (cooling). A film or convection coefficient, h , is introduced in the numerical model as a thermal material property, in addition to conductivity, specific heat and enthalpy. The associated boundary condition can be stated as

$$-k_n \frac{\partial T}{\partial n} = \sigma\varepsilon(T^4 - T_r^4) + h(T - T_\infty) \quad (8)$$

Where K_n refers to thermal conductivity normal to surface; h and ε depict surface heat transfer coefficient and emissivity respectively; σ is stefan- boltzmann constant, and T_r is the ambient temperature, T_∞ is the bulk temperature of the surrounding air. The initial condition for the transient analysis is

$$T(x, y, z, 0) = T_0 \quad (9)$$

Where T_0 is the initial temperature.

3.2 Heat Source Model

In the present model, the arc heat flux is Goldak distribution and laser heat flux is regarded as a body Gaussian distribution and a surface heat flux model that Plaser affects the effective radius of

the arc which is 10mm. The Gaussian distribution model is used to describe the laser beam body heat flux distribution, in the following form

$$q_{vlaser} = 3\eta_{lv} \frac{P_{laser}}{\pi R_l^2} \exp\left(-3 \frac{(x-x_0)^2 + (z-vt+h)^2}{R_l^2}\right) \left(\frac{y}{2L}\right) \quad (10)$$

Where η_{lv} is the efficiency of laser energy absorbed into material volume, P_{laser} is the nominal power of the laser beam, x_0 is the location of the laser head along the x-coordinate and in this study $x_0 = 127\text{mm}$, L is the thickness of the material which is 4mm, R_l is the effective radius of the laser beam, R_l is set at 0.6mm, h is the stand-off distance between the center of laser beam and the center of the electric arc and $h=2\text{mm}$. v is welding speed and t is the time of welding.

The TIG arc energy was described by a volume heat which distributes in the form of the Gaussian function along the x, y and z directions, which was given by following equation that was proposed by Goldak et al. [27]

$$q_f = \frac{6\sqrt{3}\eta_a P_{arc} f_f}{\pi\sqrt{\pi} a_f b c} \exp\left(-3 \left(\frac{x^2}{a_f^2} + \frac{y^2}{b^2} + \frac{z^2}{c^2}\right)\right)$$

$$q_r = \frac{6\sqrt{3}\eta_a P_{arc} f_r}{\pi\sqrt{\pi} a_r b c} \exp\left(-3 \left(\frac{x^2}{a_r^2} + \frac{y^2}{b^2} + \frac{z^2}{c^2}\right)\right) \quad (11)$$

Where η_a is the efficiency of arc energy absorption into the material, P_{arc} is the nominal power of the arc. The geometric parameters of Goldak distribution are illustrated in Figure 2.

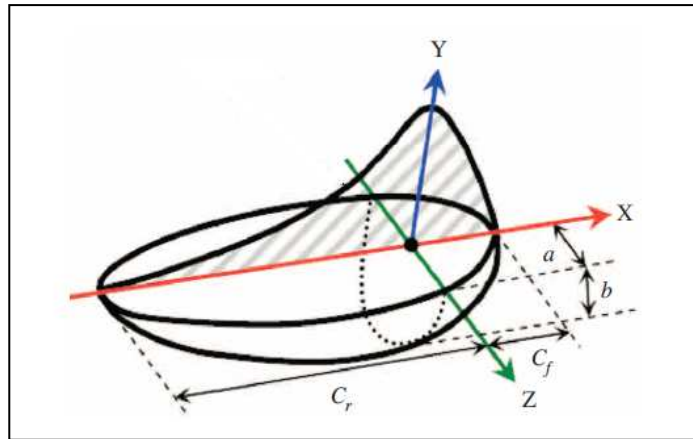


Figure2. Goldak heat source model

The Gaussian distribution model is used to describe the TIG surface heat flux distribution, in the following form

$$q_{vlaser} = 3\eta_l \frac{P_{laser}}{\pi R_l^2} \exp\left(-3 \frac{(x-x_0)^2 + (z-vt+h)^2}{R_l^2}\right) \left(\frac{y}{2L}\right) \quad (12)$$

3.3 Simulation Procedure

A 3D FE simulation of the butt joint welding has been performed on a stainless steel 1.4418 in dimensions of 127× 38× 4mm. Due to the symmetry, only one half of the plate is modeled. Accordingly, the energy meets the adiabatic condition on the symmetry surface. Geometry of the specimen was modeled at first and then the mesh was generated. Then the heat source model was simulated as described in section 3-2. Temperature field of the plate heated by the laser and tig was determined using “uncoupled heat transfer” finite element analysis in ABAQUS/Standard. The boundary and the initial conditions were applied in the form of heat loss and temperature of the environment respectively. The thermo-physical material properties incorporated in the research are presented in Table 3.

Table3. Thermo-physical properties of stainless steel 1.4418

Temperature(°K)	Specific heat (J/kg°C)	Conductivity (W/mK)
293	430	15
373	460	20
673	520	25
1073	580	35
1473	640	45

It was necessary to use a very fine mesh near the weld line in order to simulate the heat flux on the top surface and have precise results. However a coarser mesh was adopted for the region far from the weld line so that reduces the simulation time. The 8-node hexahedral elements, DC3D8 were used for these two regions. These two parts were connected with 4-node tetrahedral element, DC3D4. Comparison between computing time and accuracy leads to the final mesh size. Mesh of the model is shown in Figure 3.

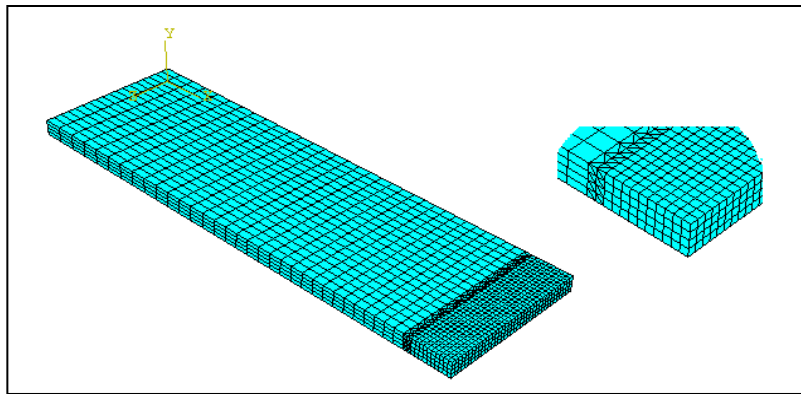


Figure3. Mesh of the model

All material properties were introduced to model as temperature dependent. The movement of the laser and TIG along the weld line was defined by time increment of step. The load of the step, which is described in the section 3.2, was programmed in FORTRAN as DFLUX subroutine. The load of former step is deleted when the heat flux moves from one time step to another. Heat transfer during this analysis is type of conduction, convection and radiation. The predefined temperature of

the work piece was 298 (°K) (the ambient temperature) and the work piece was proposed to have free convection by the air.

4. Results and discussion

Finite element simulations were carried out by FEM code ABAQUS for each condition using the geometry, mesh and the heat flux distribution described above, to determine the weld pool geometry i.e. bead width and depth of penetration. The ABAQUS program is capable of calculating the temperature at any nodal point in the material.

Figure 4 shows the temperature distribution contours in the laser-TIG hybrid welding process at instant of $t = 6.81s$. Figure5 shows the thermal analysis results (right side) and micrographs (left side) across the cross-section of the weld bead obtained by laser-TIG hybrid welding process. The process parameters are mentioned in Table 2. The counter of melting point ($1773^{\circ}K$) defines the weld pool geometry and the fusion zone. This Figure shows good accordance between numerical and experimental results.

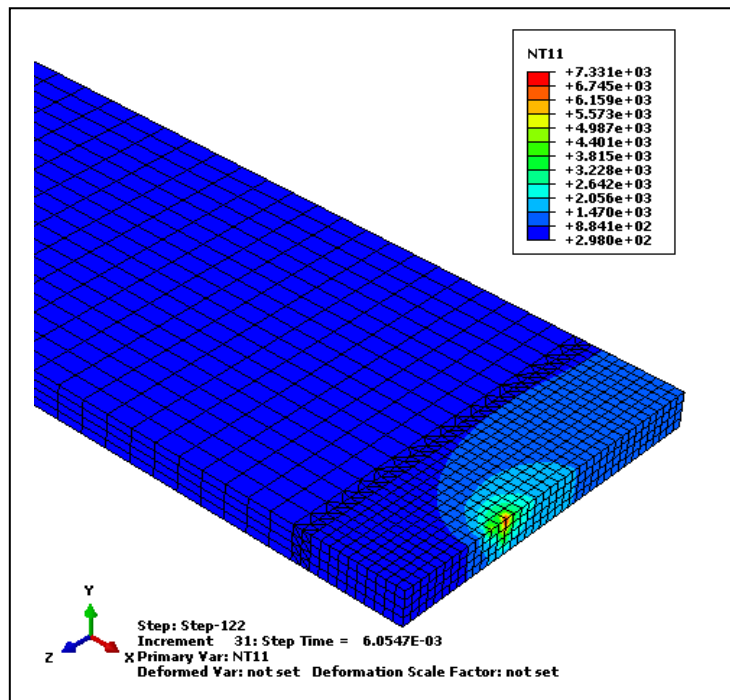


Figure4. Temperature distribution during laser-tig hybrid welding

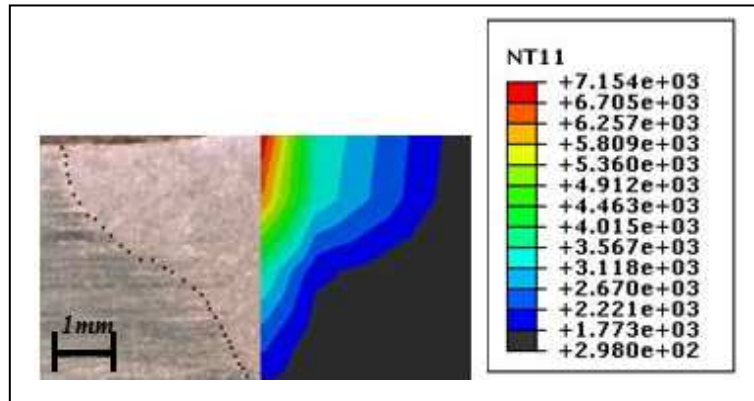


Figure5.Comparison between simulated and experimental results (Temperature unit is centigrade)

Figure 6 shows time-temperature diagram of the HLAW process at $t=6.81s$ at four points. The coordinates of these four points are; P1(127,4,15), P2(126,4,15), P3(125,4,15), P4(124,4,15), P5(123,4,15). In point number 1, the first peak of temperature is observed in 6s and it means that the arc of TIG affected there. The welding speed is 2.5mm/s and distance between laser and arc is 2mm, so the laser beam influences in this point after 0.8s, $(2(mm))/2.5(mm/s)=0.8s$. Therefore another temperature peak is observed in point 1. Point number 2, 3 and 4 are located in the fusion zone because the maximum temperature in these points is more than the melting point of the material. In point 5 the maximum temperature is less than the melting point of the material.

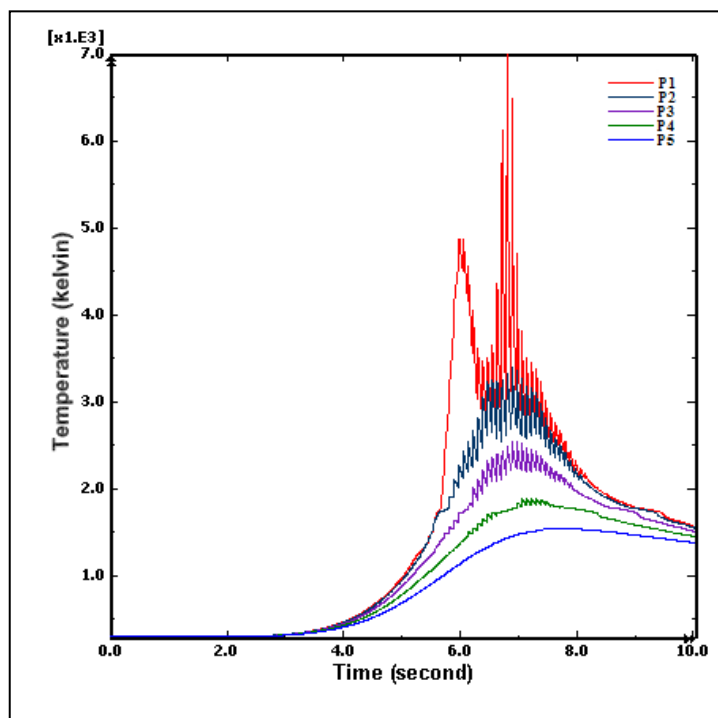


Figure6.Time-temperature diagram of the process

5. Conclusions

From finite element simulation of HLAW, the following conclusions can be drawn:

(1) Developed FEM model, due to low cost, rapid responses and high capabilities, is a suitable

method for simulating laser-TIG hybrid welding.

(2) The new developed model using the mentioned equation for temperature distribution can produce precise results for butt joint HLAW of stainless steel 1.4418.

(3) From the material properties, the conductivity of material has the most important effect on the weld bed dimensions.

6. References

- [1] Steen, W.M. 1980. Arc augmented laser processing of materials, *Journal of Applied Physics*, 51(11), 5636-5641.
- [2] Bagger, C. and Olsen, F. O. 2005. Review of laser hybrid welding. *Journal of Laser Application*, 17(1), 2-14.
- [3] Campana, G., Fortunato, A., Ascari, A., Tani, G. and Tomesani, L. 2007. The influence of arc transfer mode in hybrid laser-mig welding, *Journal of Materials Processing Technology*, 191(1-3), 111-113.
- [4] Ghosal, S. and Chaki, S. 2010. Estimation and optimization of depth of penetration in hybrid CO₂ LASER-MIG welding using ANN-optimization hybrid model, *International Journal of Advanced Manufacturing Technology*,. 47, 1149-1157.
- [5] Kim, K., Lee, J. and Cho, H. 2010. Analysis of pulsed Nd:YAG laser welding of AISI 304 steel, *Journal of Mechanical Science and Technology*, 24(11), 2253-2259.
- [6] Wang, J., Wang, C., Meng, X., Hu, X., Yu, Y. and Yu, S. 2011. Interaction between laser-induced plasma/vapor and arc plasma during fiber laser-MIG hybrid welding, *Journal of Mechanical Science and Technology*, 25(6), 1529-1533.
- [7] Hee, S., B., Han, S. B., You, C. K. and Sung, M. J. 2010. Analysis of residual stress on AH32 butt joint by hybrid CO₂ laser-GMA welding, *Computational Materials Science*, 49(2), 217-221.
- [8] Khorram, A., Ghoreishi, M., Soleymani Yazdi, M.R. and Moradi, M. 2011. Optimization of Bead Geometry in CO₂ Laser Welding of Ti 6Al 4V Using Response Surface, *Methodology Engineering*, 3, 708-712.
- [9] Moradi, M., Ghoreishi, M., Karlsson, J. and Kaplan, A.F.H. 2013. An investigation on stability of laser hybrid arc welding, *Optics and Lasers in Engineering*, 51(4), 481-487.
- [10] Javid, Y. and Ghoreishi, M. 2012. Thermo-mechanical Analysis of the LaserWelding of Stainless Steel 304, *Lasers in Engineering*, 23(1-2), 69-84.
- [11] Javid, Y., Ghoreishi, M. and Shamsaei, S. 2011. A three-dimensional heat transfer simulation of laser full penetration welding of rene-80 super alloy, *Lasers in Engineering*, 22, 1-11.
- [12] Zeng, Z., Li, X., Miao, Y., Wu, G. and Zhao, Z. 2011. Numerical and experiment analysis of residual stress on magnesium alloy and steel butt joint by hybrid laser-TIG welding, *Computational Materials Science*, 50(5), 1763–1769.
- [13] Cerit, M., Kokumer, O. and Genel, K. 2010. Stress concentration effects of undercut defect and reinforcement metal in butt welded joint, *Engineering Failure Analysis*, 17, 571–578.
- [14] Cho, W.I., Na, S.J., Cho, M.H. and Lee, J.S. 2010. Numerical study of alloying element distribution in CO₂ laser–GMA hybrid welding, *Computational Materials Science*, 49(4), 792–800.

- [15] Chen, Y.B., Lei, Z.L., Li, L.Q. and Wu, L. 2006. Experimental study on welding characteristics of CO₂ laser TIG hybrid welding process, *Science and Technology of Welding and Joining*, 11(4), 403-411.
- [16] Kong, F. and Kovacevic, R. 2010. 3D finite element modeling of the thermally induced residual stress in the hybrid laser/arc welding of lap joint, *Journal of Materials Processing Technology*, 210(6-7), 941-950.
- [17] Deng, D. 2009. FEM prediction of welding residual stress and distortion in carbon steel considering phase transformation effects, *Materials and Design*, 30, 359–366.
- [18] Khorram,A., Ghoreishi, M., Soleymani Yazdi, M.R. and Moradi, M. 2010. Using ANN Approach to Investigate the Weld Geometry of Ti 6Al 4V Titanium Alloy, *International Journal of Engineering and Technology*, 2(5), 488- 495.
- [19] Moradi, M. and Ghoreishi, M. 2011. Influences of laser welding parameters on the geometric profile of Ni-base super alloy Rene 80 weld-bead, *International Journal of Advanced Manufacturing Technology*, 55, 205–215.
- [20] Moradi, M., Salimi, N., Ghoreishi, M., Abdollahi, H., Shamsborhan, M., Frostevarg, J., Ilar, T. and Kaplan, A.F.H. 2014. Parameter dependencies in laser hybrid arc welding by design of experiments and by a mass balance, *Journal of Laser Applications*, 26(2), 022004.
- [21] Mohazab Pak, A. and Moradi, M. 2015. Hole Geometry Features Analysis in Fiber Laser Percussion Drilling Process, *International Journal of Advances in Mechanical and Automobile Engineering*, 2(1), 18-21.
- [22] Golchin, E., Moradi,M. and Shamsaei, S. 2015. Laser drilling simulation of glass by using finite element method and selecting the suitable Gaussian distribution. *Modares Mechanical Engineering, Proceedings of the Advanced Machining and Machine Tools Conference*, 15(13), 416-420. (In Persian)
- [23] Moradi, M., Ghoreishi, M. and Torkamany, M.J. 2014. Modeling and Optimization of Nd:YAG Laser-TIG Hybrid Welding of Stainless Steel, *Journal of lasers in Engineering*, 27(3-4), 211–230.
- [24] Moradi, M., Ghoreishi, M., Torkamany, M.J., Sabbaghzadeh, J. and Hamedi, M.J. 2012. An Investigation on the effect of pulsed Nd:YAG laser welding parameters of stainless steel 1.4418, *Advanced Materials Research*, 383, 6247-6251.
- [25] Magee, K.H., Merchant,V.E. and Hyatt, C.V. 1990. Laser assisted gas metal arc weld characteristics. presented at the 1990 international symposium on application of lasers and electro-optics (ICALEO 90) and to be published in the conference proceeding.
- [26] Krutz, G.W. and Segerlind, L.J. 1978. Finite element analysis of weld structures, *Welding Journal Research Supplement*, 57, 211-216.
- [27] Goldak, J., Chakravarti, A. and Bibby, M. 1984. A New Finite Element Model for Welding Heat Sources, *Metallurgical Transactions B*, 15B, 299-305.